metals

MDPI

Article

First-Principles Study of Cu Addition on Mechanical Properties of Ni_3Sn_4-Based Intermetallic Compounds

Jinye Yao [1], Li Wang [1], Shihao Guo [1], Xiaofu Li [1], Xiangxu Chen [1], Min Shang [1], Haoran Ma [2] and Haitao Ma [1,*]

[1] School of Materials Science and Engineering, Dalian University of Technology, Dalian 116000, China; yaojinye@mail.dlut.edu.cn (J.Y.); brose2wang@mail.dlut.edu.cn (L.W.); 1244250146@mail.dlut.edu.cn (S.G.); lixiaofu@mail.dlut.edu.cn (X.L.); xiangxuchen@mail.dlut.edu.cn (X.C.); shangxiaomin2019@mail.dlut.edu.cn (M.S.)

[2] School of Microelectronics, Dalian University of Technology, Dalian 116024, China; mhr@dlut.edu.cn

* Correspondence: htma@dlut.edu.cn

Abstract: Ni–Cu under-bump metallisation (UBM) can reduce stress and improve wetting ability in technology for electronic packaging technology advances with three-dimensional integrated circuit (3D IC) devices. The bond between the Sn-based solder and Ni–Cu UBM is affected by the formation of intermetallic compounds (IMCs), specifically Ni_3Sn_4 and $(Ni,Cu)_3Sn_4$. This paper investigates the mechanical properties of IMCs, which are critical in assessing the longevity of solder joints. First-principles calculations were carried out to investigate the phase stability, mechanical properties and electronic structures of Ni_3Sn_4, $Ni_{2.5}Cu_{0.5}Sn_4$, $Ni_{2.0}Cu_{1.0}Sn_4$, and $Ni_{1.5}Cu_{1.5}Sn_4$ IMCs. The calculated formation enthalpies show that the doping of Cu atoms leads to a decrease in the stability of the phases and a reduction in the mechanical properties of the Ni_3Sn_4 crystal structure. As the concentration of Cu atoms in the Ni_3Sn_4 cells increases, the bulk modulus values of $(Ni,Cu)_3Sn_4$ formed with different compositions decrease from 107.78 GPa to 87.84 GPa, the shear modulus decreases from 56.64 GPa to 45.08 GPa, and the elastic modulus decreases from 144.59 GPa to 115.48 GPa, indicating that the doping of Cu atoms into the Ni_3Sn_4 cells may adversely affect their mechanical properties and increase the possibility of microcracking at the interface during actual service. The anisotropy of $(Ni,Cu)_3Sn_4$ is more significant than that of Ni_3Sn_4, with $Ni_{2.0}Cu_{1.0}Sn_4$ showing the highest anisotropy. After evaluating the electronic structures, the metallic properties of Ni_3Sn_4 and the $Ni_{2.5}Cu_{0.5}Sn_4$, $Ni_{2.0}Cu_{1.0}Sn_4$, and $Ni_{1.5}Cu_{1.5}Sn_4$ phases are revealed by electronic structure analysis. The total density of states (TDOS) for $(Ni,Cu)_3Sn_4$ structures is mainly influenced by Ni-d and Cu-d states. The addition of Cu atoms can increase the brittleness of Ni_3Sn_4. In addition, the region where d and p hybridisation occurs gradually increases with increasing Cu content. The electronic properties suggest that the binding energy between Ni and Sn atoms weakens with the addition of Cu atoms, resulting in a decrease in the elastic modulus. This research can serve as a valuable reference and theoretical guide for future applications of these materials.

Keywords: intermetallic compounds; first-principles calculations; mechanical properties; electronic structures

Citation: Yao, J.; Wang, L.; Guo, S.; Li, X.; Chen, X.; Shang, M.; Ma, H.; Ma, H. First-Principles Study of Cu Addition on Mechanical Properties of Ni_3Sn_4-Based Intermetallic Compounds. *Metals* **2024**, *14*, 64. https://doi.org/10.3390/met14010064

Academic Editor: Emin Bayraktar

Received: 1 December 2023
Revised: 31 December 2023
Accepted: 3 January 2024
Published: 5 January 2024

1. Introduction

Three-dimensional electronic packaging technology can meet the high-density assembly performance requirements of today's electronic products while also providing high reliability, fast transmission speeds, low power consumption, low cost, and light weight [1–3]. At the same time, there can be concerns about the reliability of solder joints as they become smaller and smaller [4]. The reliability of microelectronic brazed interconnects is primarily influenced by the wetting behaviour of the solder bump, as well as the interfacial reactions between the solder and the metal layer beneath the bump during production and service, and electron migration. The bonding of the Sn-based solder/UBM interface during the soldering process is influenced by the physicochemical properties of

the interacting materials, in particular the diffusion process and the resulting formation of various intermetallic compounds (IMCs) [5,6]. Meanwhile, the changes in the interfacial microstructure and mechanical properties of solder joints are usually the cause of serious reliability problems. Thick IMC layers have been found to weaken the mechanical properties and cause reliability problems, while thin IMC layers can increase the strength of the joint [7]. As the demand for smaller electronic devices increases, solder joints are shrinking in size. This decrease in solder volume increases the volume fraction of IMCs in the total solder joint volume, making the interface behaviour more important. In fact, the mechanical properties of IMCs largely determine the failure mechanisms of solder joints, which have emerged as a critical issue in solder reliability [8–10]. Therefore, it is crucial to understand the mechanical properties of IMCs in order to assess the reliability of solder joints in electronic packaging.

For example, due to the difference in ductility between the IMC layer and substrate, the stress distribution within solder joints is altered during reflow and ageing. To achieve slower reaction rates or more stable IMCs, the composition of UBM films can be adjusted. Compared to copper (Cu) UBM, nickel (Ni) UBM exhibits a reduced interfacial reaction with solders, as shown in previous research [11–14]. Ni and Ni-based alloys are known to have favourable magnetic properties, excellent mechanical properties and excellent corrosion and abrasion resistance. A variety of Ni-based UBMs have been used in industry to improve reliability [15]. These include widely used UBMs such as electroplated Ni, sputtered Ni(V) and electroless Ni(P)/Au. However, Ni UBM has a notable disadvantage in the form of inherent stress generation during the plating process [16,17]. After investigating the detrimental effects of Ni film and considering the potential of Ni–Cu to reduce stress and improve wetting, the use of Ni–Cu UBM as a replacement for Ni UBM is a viable option.

For this reason, interfacial reactions and IMC growth between Sn-based and Ni–Cu substrates have been the subject of much interest. Sn-based solders react with Ni coatings, primarily forming the intermetallic compound Ni_3Sn_4 [18–20]. In addition, Sn–Ag–Cu ternary lead-free solders are considered to be some of the best candidates for replacing conventional Sn–Pb solders in electronic packaging due to their desirable properties. It has also been observed by other researchers that Cu atoms can also replace Ni atoms in sublattice positions of Ni_3Sn_4 to form a ternary intermetal, $(Ni,Cu)_3Sn_4$. It is possible that the mechanical properties of Ni_3Sn_4 can be altered by doping with Cu atoms. However, most research on $(Ni,Cu)_3Sn_4$ has been experimental. Few studies have focused on the mechanical properties of $(Ni,Cu)_3Sn_4$ [21,22]. Further studies are needed to investigate the stability of $(Ni,Cu)_3Sn_4$ in more detail. The initial stage of first-principles calculations involves identifying the most stable geometric structure corresponding to the lowest energy, as well as determining the electronic, thermodynamic, and optical properties of a material through self-consistent calculations based on the laws of quantum mechanics and its constituent atoms [23,24]. In this paper, first-principles calculations are used as a convenient scheme to derive the essential properties of materials. The effect of Cu additions on the mechanical properties of Ni_3Sn_4 IMCs is investigated in this work. We will perform first-principles calculations on Ni_3Sn_4, $Ni_{2.5}Cu_{0.5}Sn_4$, $Ni_{2.0}Cu_{1.0}Sn_4$, and $Ni_{1.5}Cu_{1.5}Sn_4$ to derive their structural, elastic, thermodynamic and electronic properties. The results of our systematic research will complement the physical property data and facilitate the discovery of intermetallic structural stability and mechanical properties.

2. First-Principles Calculation Details

The initial model for this study was taken from the experimental crystal structure of Ni_3Sn_4 [25]. Figure 1a shows the primitive structure of the Ni_3Sn_4 phase, which was a monoclinic structure in the C2/m space group and contained six Ni and eight Sn atoms per cell. It can be seen that the Ni atoms occupy two different positions, 2a (Ni_1) and 4i (Ni_2). Ni_1 is located at the eight top angles of the hexahedron and the face centre position of the xy plane, while Ni_2 is located in the interior of the hexahedron and the xz plane [26]. The formation enthalpy calculations show that $Ni_{2.5}Cu_{0.5}Sn_4$(2a) has a value of

−219.65 meV/atom and $Ni_{2.5}Cu_{0.5}Sn_4$ (4i) has a value of −226.19 meV/atom. This suggests that Cu has a greater tendency to occupy the 4i site [27]. In this paper, only the substitution of the Ni 4i position is discussed. It was found that during reflow and ageing, the diffusion of Cu atoms to the interface gradually decreases with the increasing addition of Ni. When using SAC-1Ni as the soldering material, the resulting IMC $(Ni,Cu)_3Sn_4$ contains 10.17–27.2% Cu [28,29]. According to the formulas of $Ni_{2.5}Cu_{0.5}Sn_4$, $Ni_{2.0}Cu_{1.0}Sn_4$ and $Ni_{1.5}Cu_{1.5}Sn_4$, different amounts of Cu (7.14 at.%, 14.3 at.% and 21.4 at.%, respectively) were added to the Ni_3Sn_4 phase, which are shown in Figure 1b–d.

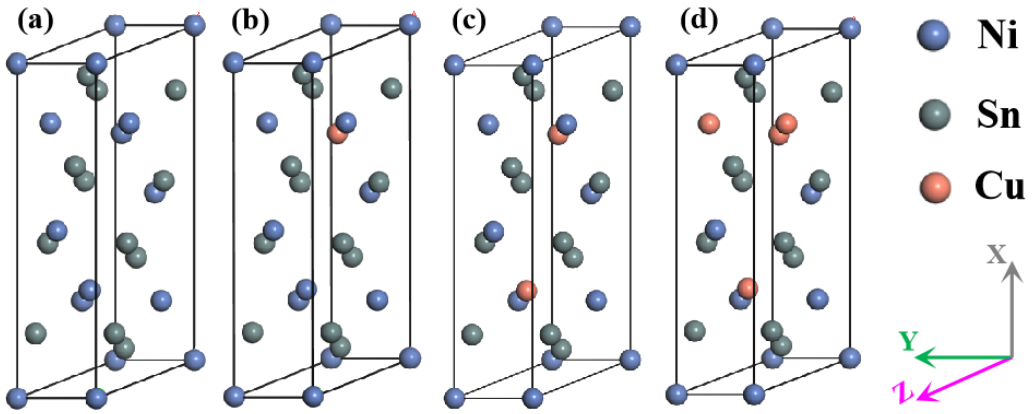

Figure 1. Crystal structures of (**a**) Ni_3Sn_4, (**b**) $Ni_{2.5}Cu_{0.5}Sn_4$, (**c**) $Ni_{2.0}Cu_{1.0}Sn_4$, (**d**) $Ni_{1.5}Cu_{1.5}Sn_4$.

In this study, first-principles calculations using density functional theory (DFT) were performed using the Cambridge Sequential Total Energy Package (CASTEP, 2017, Dassault Systèmes is located in Paris, France) [30]. To ensure the accuracy of subsequent calculations and to obtain the most stable crystal structure, strict total energy convergence tests were implemented. An energy threshold of 400 eV and 3 × 9 × 7 Monkhorst-Pack k-points were used to calculate the lattice parameters and elastic constants (C_{ij}) for the Ni_3Sn_4, $Ni_{2.5}Cu_{0.5}Sn_4$, $Ni_{2.0}Cu_{1.0}Sn_4$, and $Ni_{1.5}Cu_{1.5}Sn_4$ phases.

The Generalised Gradient Approximation (GGA) was used to treat the exchange and correlation function in terms of the Perdew–Burke–Ernzerhof (PBE) exchange–correlation energy [31]. The stability of intermetallic compounds can be determined by comparing their formation energies. In general, a compound will only form if its energy is less than the sum of the energies of the individual crystals. Therefore, the more negative the formation energy, the more stable the resulting compound will be. In order to study the thermodynamic stability, the heats of formation for Ni_3Sn_4, $Ni_{2.5}Cu_{0.5}Sn_4$, $Ni_{2.0}Cu_{1.0}Sn_4$, and $Ni_{1.5}Cu_{1.5}Sn_4$ were calculated using the following formula:

$$\Delta H = E_{total}(Ni_xCu_ySn_z) - [xE_{total}(Ni) + yE_{total}(Cu) + zE_{total}(Sn)] \quad (1)$$

in which $E_{total}(Ni_xCu_ySn_z)$ is the calculated total energy of $Ni_xCu_ySn_z$ at equilibrium lattice constants. The energies of the isolated Ni, Cu and Sn atoms are given as $E_{total}(Ni)$, $E_{total}(Cu)$and $E_{total}(Sn)$, respectively. In $Ni_xCu_ySn_z$, x, y and z denote the number of Ni, Cu and Sn atoms, respectively.

3. Results and Discussion

3.1. Structure Optimisation

For Ni_3Sn_4, $Ni_{2.5}Cu_{0.5}Sn_4$, $Ni_{2.0}Cu_{1.0}Sn_4$, and $Ni_{1.5}Cu_{1.5}Sn_4$, the optimised structural parameters calculated are shown in Table 1. These results are discussed in this paper along with other literature [26,32,33]. Our analysis showed that the structural parameters calculated in this work have minimal deviations from the existing literature, and the deviations are less than 1.0%. This demonstrates the validity of the theoretical approaches used. It was observed that the lattice constants remained largely unaffected by the addition

of Cu to all phases. This indicates that there were no changes in the crystal structures following the introduction of Cu atoms into the Ni_3Sn_4 phase. To determine the effect of Cu additions on the phase stability of Ni_3Sn_4, the heat of formation (ΔH, meV/atom) for Ni_3Sn_4, $Ni_{2.5}Cu_{0.5}Sn_4$, $Ni_{2.0}Cu_{1.0}Sn_4$, and $Ni_{1.5}Cu_{1.5}Sn_4$ at zero temperature, we calculated the heat of formation using Equation (1). The results are given in Table 1. A negative ΔH indicates the stability of the studied phase and a larger negative energy implies a more stable structure. The heat of formation of Ni_3Sn_4 in this work was −284 meV/atom, close to the previously calculated results of −260, −267, and −269 meV/atom. As shown in Figure 2, when Cu atoms were added to the Ni_3Sn_4 structure, the heat of formation increased slightly, with ΔH = −248 meV/atom for $Ni_{2.5}Cu_{0.5}Sn_4$, ΔH = −205 meV/atom for $Ni_{2.0}Cu_{1.0}Sn_4$, and ΔH = −165 meV/atom for $Ni_{1.5}Cu_{1.5}Sn_4$. The structure of Ni_3Sn_4 was found to be more stable than that of $(Ni,Cu)_3Sn_4$ IMCs. In simple terms, the introduction of Cu atoms reduced the structural integrity of the Ni_3Sn_4 IMC. Increasing the number of Cu atoms leads to a decrease in the stability of the structure.

Table 1. The lattice constants *a*, *b* and *c* (Å), angle β (°) and the heat of formation (ΔH, meV/atom) of Ni_3Sn_4, $Ni_{2.5}Cu_{0.5}Sn_4$, $Ni_{2.0}Cu_{1.0}Sn_4$, and $Ni_{1.5}Cu_{1.5}Sn_4$ obtained from Refs. [26,27,32,33] and this paper.

Phases	Reference	*a*	*b*	*c*	β	ΔH
Ni_3Sn_4	This work	12.323	4.119	5.303	105.416	−284
	[26]	12.299	4.084	5.288	105.190	−260
	[32]	12.418	4.111	4.315	105.480	−267
	[33]	12.334	4.100	5.325	105.010	−269
$Ni_{2.5}Cu_{0.5}Sn_4$	This work	12.419	4.146	5.291	105.555	−248
	[26]	12.357	4.102	5.307	105.150	−219
	[32]	12.426	4.101	5.363	105.690	−193
$Ni_{2.0}Cu_{1.0}Sn_4$	This work	12.434	4.149	5.365	105.541	−205
	[26]	12.420	4.128	5.331	105.150	−179
	[27]	12.422	4.133	5.331	105.160	−188
$Ni_{1.5}Cu_{1.5}Sn_4$	This work	12.538	4.173	5.382	105.958	−165
	[26]	12.495	4.145	5.381	105.16	−135
	[27]	12.507	4.146	5.382	105.07	−144

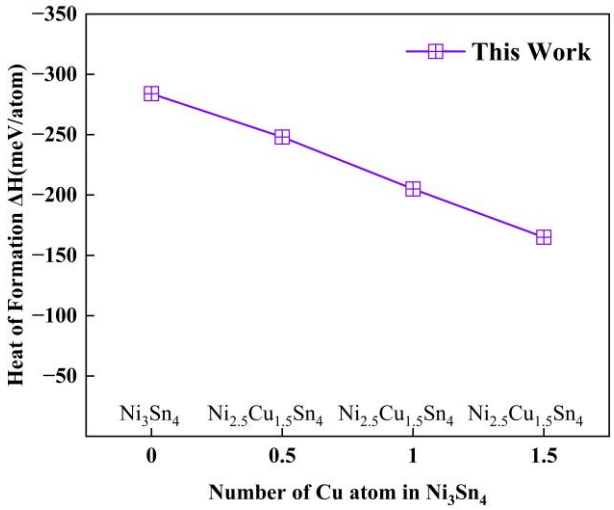

Figure 2. The variation of the heat of formation (ΔH, meV/atom) with the Cu atom fraction.

3.2. Mechanical Properties

This study investigates the effect of Cu addition on the mechanical properties of Ni_3Sn_4. The elastic constant (C_{ij}) of Ni_3Sn_4-based structures was calculated. The elastic constant (C_{ij}) characterises the elasticity of a material and is represented by the quadratic coefficient

in the case of small strains [34]. The matrix of elastic constants can be summarised in 13 variables, based on the symmetry of monoclinic structures [35].

The C_{ij} results obtained are listed in Table 2. The mechanical stability of the crystal structure could be determined by using independent elastic constants, while for a monoclinic structure composed of Ni_3Sn_4-based IMCs, the conditions required for mechanical stability can be defined as follows:

$$C_{ii} > 0 (i = 1–6) \tag{2}$$

$$[C_{11} + C_{22} + C_{33} + 2(C_{12} + C_{13} + C_{23})] > 0 \tag{3}$$

$$(C_{33}C_{55} - {C_{35}}^2) > 0, (C_{44}C_{66} - {C_{46}}^2) > 0, (C_{22} + C_{33} - 2C_{23}) > 0 \tag{4}$$

Table 2. The calculated elastic constants C_{ij} (GPa) for Ni_3Sn_4, $Ni_{2.5}Cu_{0.5}Sn_4$, $Ni_{2.0}Cu_{1.0}Sn_4$, and $Ni_{1.5}Cu_{1.5}Sn_4$ obtained from Refs. [26,32,33] and this paper.

Phases	Reference	C_{11}	C_{12}	C_{13}	C_{22}	C_{23}	C_{33}	C_{44}	C_{55}	C_{66}	C_{15}	C_{25}	C_{35}	C_{46}
Ni_3Sn_4	This work	165.96	74.58	72.13	183.59	68.85	191.67	62.35	64.28	55.35	−17.26	12.83	−5.70	9.67
	[26]	176.60	64.30	57.40	146.00	76.10	169.70	60.80	49.50	46.70	−22.90	7.00	−9.60	6.90
	[32]	155.48	70.68	69.34	164.33	68.26	149.86	62.74	59.99	59.95	−21.97	13.99	−8.73	4.90
	[33]	153.09	68.22	63.25	144.31	75.37	176.53	57.42	57.35	53.84	−22.70	12.94	−11.11	9.09
$Ni_{2.5}Cu_{0.5}Sn_4$	This work	153.70	67.24	63.10	165.94	63.53	186.08	48.84	59.64	57.98	−21.22	12.00	−4.30	9.61
	[32]	146.95	71.79	64.07	176.30	73.29	154.47	57.86	55.11	55.41	−21.79	11.93	−6.18	8.22
$Ni_{2.0}Cu_{1.0}Sn_4$	This work	138.64	63.51	62.15	156.72	60.21	166.06	45.23	47.76	56.05	−20.92	10.26	−4.43	8.55
$Ni_{1.5}Cu_{1.5}Sn_4$	This work	134.58	53.68	59.37	146.62	69.75	148.91	54.13	40.93	55.57	−14.66	8.82	−4.51	7.93

Table 2 shows the calculated elastic constants (C_{ij}) for all Ni_3Sn_4-based structures. The elastic constants (C_{ij}) of Ni_3Sn_4 are close to the other calculations [26,32,33]. C_{11} represents the elastic deformation resistance of the crystal structures in the [100] direction [36]. It can be observed that the value of C_{11} for Ni_3Sn_4 is 165.96 GPa, which is higher than that of $(Ni,Cu)_3Sn_4$. This suggests that Ni_3Sn_4 exhibits the highest resistance to elastic deformation. From Table 2, the elastic constants (C_{ij}) were calculated for all the Ni_3Sn_4-based structures; $(Ni,Cu)_3Sn_4$ structures typically have lower elastic constants (C_{ij}) than Ni_3Sn_4. And the corresponding criteria listed in Equations (2)–(4) were easily satisfied, indicating that the Ni_3Sn_4-based structures studied are mechanically stable at 0 K.

In order to further approximate the Young modulus of Ni_3Sn_4-based ternary structures in the polycrystalline state [37], Voight–Reuss–Hill (VRH) [38] can be applied. The Voigt (V) and Reuss (R) for bulk and shear modulus can be calculated as follows:

$$B_V = \frac{1}{9}[C_{11} + C_{22} + C_{33} + 2(C_{12} + C_{13} + C_{23})] \tag{5}$$

$$G_V = \frac{1}{15}[C_{11} + C_{22} + C_{33} + 3(C_{44} + C_{55} + C_{66}) - (C_{12} + C_{13} + C_{23})] \tag{6}$$

$$B_R = \Omega \left[\begin{array}{l} a(C_{11} + C_{22} - 2C_{12}) + b(2C_{12} - 2C_{11} - C_{23}) + c(C_{15} - 2C_{25}) + \\ d(2C_{12} + 2C_{23} - C_{13} - 2C_{22}) + 2e(C_{25} - C_{15}) + f \end{array} \right]^{-1} \tag{7}$$

$$G_R = 15 \left\{ 4 \left[\frac{\begin{array}{l} a(C_{11} + C_{22} + C_{12}) + b(C_{11} - C_{12} - C_{23}) \\ +c(C_{15} + C_{25}) + d(C_{22} - C_{12} - C_{23} - C_{13}) \\ +e(C_{15} - C_{25}) + f \end{array}}{\Omega} \right] + 3 \left[\frac{g}{\Omega} + \frac{(C_{44} + C_{66})}{(C_{44}C_{66} - {C_{46}}^2)} \right] \right\}^{-1} \tag{8}$$

$$a = C_{33}C_{55} - C_{35}^2 \tag{9}$$

$$b = C_{23}C_{55} - C_{25}C_{35} \tag{10}$$

$$c = C_{13}C_{35} - C_{15}C_{33} \tag{11}$$

$$d = C_{13}C_{55} - C_{15}C_{35} \tag{12}$$

$$e = C_{13}C_{25} - C_{15}C_{23} \tag{13}$$

$$f = C_{11}(C_{22}C_{55} - C_{25}^2) - C_{12}(C_{12}C_{55} - C_{15}C_{25}) + C_{15}(C_{12}C_{25} - C_{15}C_{22}) + C_{25}(C_{23}C_{35} - C_{25}C_{33}) \tag{14}$$

$$\Omega = 2\begin{bmatrix} C_{15}C_{25}(C_{33}C_{12} - C_{13}C_{23}) + C_{15}C_{35}(C_{22}C_{13} - C_{12}C_{23}) \\ +C_{25}C_{35}(C_{11}C_{23} - C_{12}C_{13}) - C_{15}^2(C_{22}C_{33} - C_{23}^2) \\ +C_{25}^2(C_{11}C_{33} - C_{13}^2) + C_{35}^2(C_{11}C_{22} - C_{12}^2) \end{bmatrix} + gC_{55} \tag{15}$$

The following equations were used to calculate the bulk modulus (B), shear modulus (G), Young modulus (E) and Poisson ratio (ν). where B_V, B_R, G_V and G_R are the bulk and shear modulus in VRH.

$$B = \frac{(B_V + B_R)}{2} \tag{16}$$

$$G = \frac{(G_V + G_R)}{2} \tag{17}$$

$$E = \frac{9BG}{(3B + G)} \tag{18}$$

$$v = \frac{(3B - 2G)}{[2(3B + G)]} \tag{19}$$

The values for B, G, E, ν and B/G of Ni_3Sn_4-based IMCS can be obtained using Equations (16)–(19). The results are shown in Figure 3 and Table 3. The B, G, E, ν and B/G of Ni_3Sn_4 are 107.78 GPa, 56.64 GPa, 144.59 GPa, 0.276 and 1.90, respectively, which are close to the results of other references.

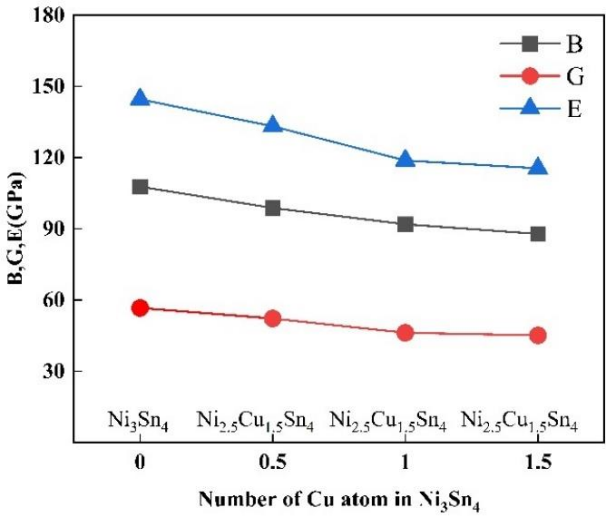

Figure 3. The variation of bulk modulus, shear modulus, and Young modulus with the Cu atom fraction.

Table 3. The calculated bulk modulus (B, GPa), shear modulus (G, GPa), Young modulus (E, GPa) and Poisson ratio (ν) for Ni_3Sn_4, $Ni_{2.5}Cu_{0.5}Sn_4$, $Ni_{2.0}Cu_{1.0}Sn_4$, and $Ni_{1.5}Cu_{1.5}Sn_4$ obtained from Refs. [23,26,27,32,33] and this paper.

Phases	Reference	*B*	*G*	*E*	*ν*	*B*/*G*
Ni_3Sn_4	This work	107.78	56.64	144.59	0.276	1.90
	[23]	102.10	54.10	127.20	0.250	1.89
	[26]	97.90	49.08	126.11	0.285	2.00
	[32]	98.01	53.96	136.78	0.287	1.82
	[33]	98.30	49.27	126.65	0.290	2.00
$Ni_{2.5}Cu_{0.5}Sn_4$	This work	98.79	52.23	133.21	0.275	1.89
	[27]	94.25	49.07	125.43	0.278	1.92
	[32]	98.45	49.62	127.45	0.284	1.95
$Ni_{2.0}Cu_{1.0}Sn_4$	This work	91.93	46.24	118.80	0.285	1.99
$Ni_{1.5}Cu_{1.5}Sn_4$	This work	87.84	45.08	115.48	0.281	1.95

Bulk modulus values for different compositions are documented as 107.78 GPa (Ni_3Sn_4), 98.79 GPa ($Ni_{2.5}Cu_{0.5}Sn_4$), 91.93 GPa ($Ni_{2.0}Cu_{1.0}Sn_4$), and 87.84 GPa ($Ni_{1.5}Cu_{1.5}Sn_4$). In addition, the shear modulus and Young modulus of Ni_3Sn_4 were 56.64 GPa and 144.59 GPa, respectively. After the addition of Cu to the Ni_3Sn_4 structure, the shear modulus and Young's modulus were significantly reduced. It can be observed that Cu addition had a significant effect on the mechanical properties of the studied Ni_3Sn_4-based alloys. For $Ni_{2.5}Cu_{0.5}Sn_4$, the values were G = 52.23 GPa and E = 133.21 GPa; for $Ni_{2.0}Cu_{1.0}Sn_4$, the values were G = 46.24 GPa and E = 118.80 GPa; and for $Ni_{1.5}Cu_{1.5}Sn_4$, the values were G = 45.08 GPa and E = 115.48 GPa. The incorporation of Cu atoms into Ni_3Sn_4 crystals is predicted to reduce the binding energy in structures containing Ni_3Sn_4. This could lead to a lower shear modulus and Young modulus.

According to Pugh's criterion [39], the B/G ratio is proposed as a condition to distinguish between brittle and ductile materials. If the value exceeds 1.75, the material has ductile properties, otherwise it is brittle. The B/G ratios for Ni_3Sn_4, $Ni_{2.5}Cu_{0.5}Sn_4$, $Ni_{2.0}Cu_{1.0}Sn_4$, and $Ni_{1.5}Cu_{1.5}Sn_4$ are 1.90, 1.89, 1.99 and 1.95, respectively. Therefore, all phases based on Ni_3Sn_4 can be classified as ductile, with the Ni_3Sn_4 IMC exhibiting the highest ductility of all the structures investigated. In addition, the Poisson ratio (ν) can be considered as a parameter to represent the ductile or brittle behaviour of materials when ν is above or below 0.25 [40].

From the Poisson ratio shown in Table 3, it was expected that all phases based on Ni_3Sn_4 would exhibit ductility. It is possible to predict the Young modulus of IMCs using first-principles calculations. Nevertheless, the plastic properties of materials are influenced by various factors such as crystal structure, microstructure and experimental conditions. It is widely accepted that material mechanics are strongly influenced by the growth and progression of microcracks. During the manufacture and use of solder joints, the anisotropic plastic deformation of intermetallic compounds leads to the formation of microcracks, which affect the reliability of electronic products [41]. To investigate the effect of the introduction of Cu on the elastic anisotropy of a Ni_3Sn_4 IMC, the universal anisotropy index (A^U) was used. A higher value of A^U indicates a greater structural anisotropy of the materials.

A^U could be expressed as the following:

$$A^U = 5\frac{G_V}{G_R} + \frac{B_V}{B_R} - 6 > 0 \quad (20)$$

If A^U has a value of zero, a crystal structure should be isotropic. A higher value of A^U indicates greater anisotropy for a material. The values of A^U for Ni_3Sn_4-based IMCs can be obtained using Equation (20). The results are given in Figure 4 and Table 4. The atomic unit (A^U) of Ni_3Sn_4 is 0.271, which is close to other references. Obviously, both Ni_3Sn_4 and $(Ni,Cu)_3Sn_4$ must be considered anisotropic materials. The addition of copper

would increase the mechanical anisotropy of the Ni_3Sn_4 intermetallic compound. The increase in elastic anisotropy resulted in a greater propensity for microcracking in Ni_3Sn_4, which reduced the shear strength of brazed joints. In order to gain further insight into the elastic anisotropy of Ni_3Sn_4-based phases, 3D surface plots of the bulk modulus and Young modulus were made in the present study.

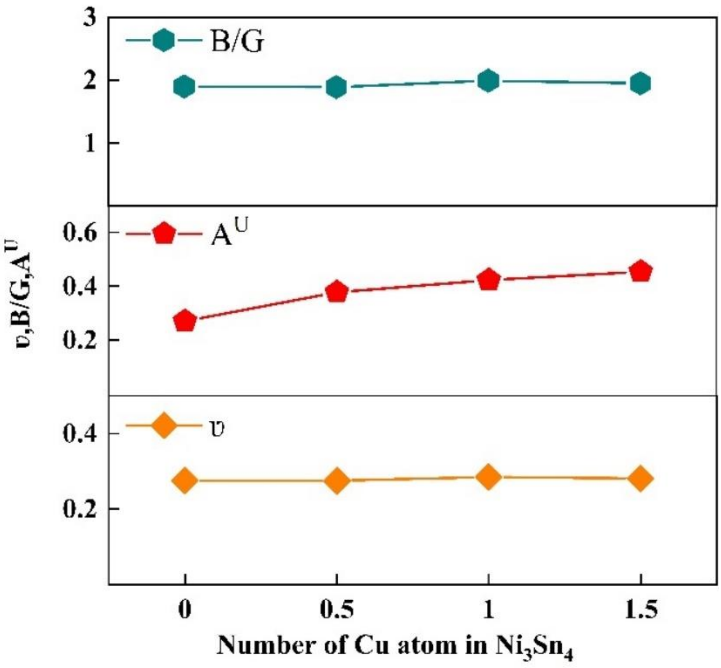

Figure 4. The variation of ν, A^U, and B/G with the Cu atom fraction.

Table 4. The calculated bulk modulus (GPa) and shear modulus (Gpa) in VRH approximations and the universal anisotropy index (A^U) for Ni_3Sn_4, $Ni_{2.5}Cu_{0.5}Sn_4$, $Ni_{2.0}Cu_{1.0}Sn_4$, and $Ni_{1.5}Cu_{1.5}Sn_4$ obtained from Refs. [32,33] and this paper.

IMCs	Reference	G_V	G_R	B_V	B_R	G_V/G_R	B_V/B_R	A^U
Ni_3Sn_4	This work	58.11	55.17	108.04	107.53	1.053	1.005	0.271
	[32]	53.96	49.42	98.47	97.56	1.092	1.001	0.461
	[33]	51.79	46.74	99.07	97.53	1.108	1.016	0.556
$Ni_{2.5}Cu_{0.5}Sn_4$	This work	54.08	50.38	99.27	98.31	1.077	1.010	0.378
	[32]	51.58	47.66	99.56	97.33	1.082	1.013	0.423
$Ni_{2.0}Cu_{1.0}Sn_4$	This work	48.18	44.30	92.57	91.28	1.088	1.014	0.454
$Ni_{1.5}Cu_{1.5}Sn_4$	This work	46.61	43.54	88.41	87.26	1.071	1.013	0.366

As shown in Figure 5, the ability of a material to resist deformation is expressed by its bulk modulus, B, which is determined by the strength and compressibility of the chemical bonds. The higher the bulk modulus of a material, the higher the corresponding strength of the material. Where the greater deviation from the spherical shape indicates greater anisotropy, it can be seen that the bulk modulus anisotropy of $(Ni,Cu)_3Sn_4$ is overall greater than that of undoped Ni_3Sn_4 as the copper atom content increases. As indicated in Figure 6, it was observed that for all structures based on Ni_3Sn_4, 3D surface plots displayed some deviations from a spherical shape. This is indicative of the elastic anisotropies of Ni_3Sn_4 and $(Ni,Cu)_3Sn_4$. Moreover, after the Cu doping, the shape of the directional modulus was further away from the sphere, indicating the stronger elastic anisotropy of $(Ni,Cu)_3Sn_4$. And the $Ni_{2.0}Cu_{1.0}Sn_4$ had the strongest anisotropy.

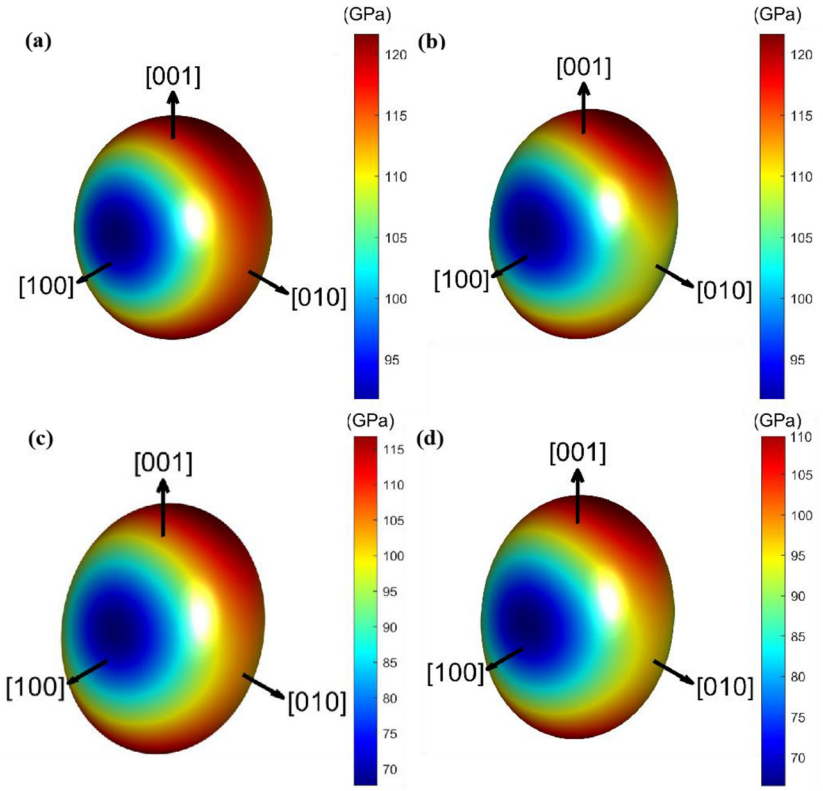

Figure 5. The surface constructions of bulk modulus for (**a**) Ni_3Sn_4, (**b**) $Ni_{2.5}Cu_{0.5}Sn_4$, (**c**) $Ni_{2.0}Cu_{1.0}Sn_4$, (**d**) $Ni_{1.5}Cu_{1.5}Sn_4$.

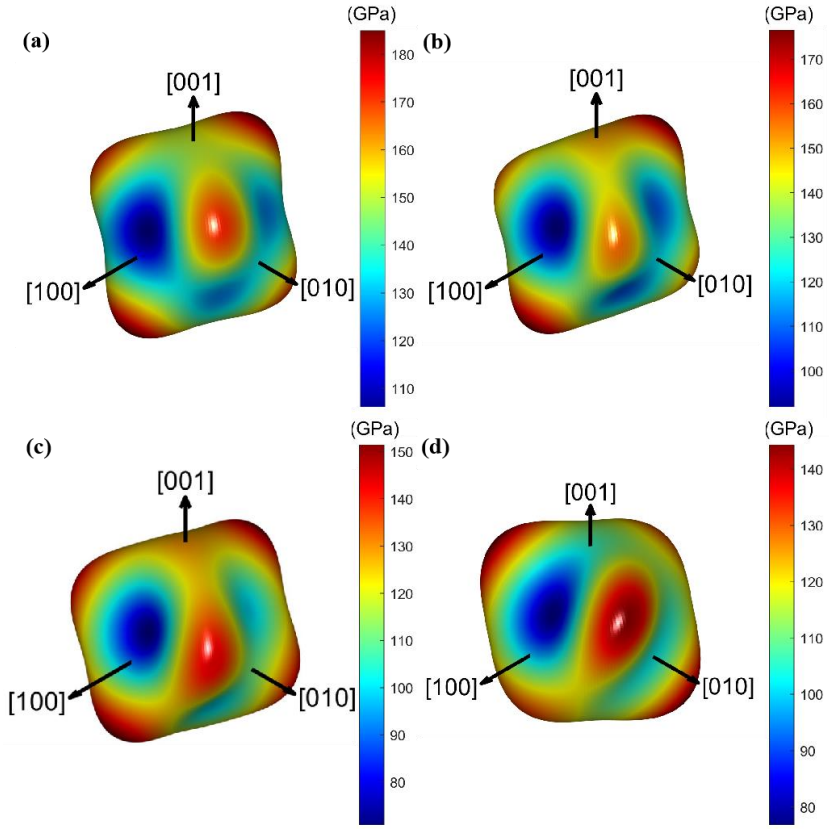

Figure 6. The surface constructions of Young modulus for (**a**) Ni_3Sn_4, (**b**) $Ni_{2.5}Cu_{0.5}Sn_4$, (**c**) $Ni_{2.0}Cu_{1.0}Sn_4$, (**d**) $Ni_{1.5}Cu_{1.5}Sn_4$.

3.3. Electronic Structures

The stability and bonding characteristics of a material are closely related to its electronic structure. In order to reveal the fundamental chemical bonding of the Ni_3Sn_4-based IMCs, the total density of states (TDOS) and partial density of states (PDOS) were performed and are shown in Figure 7. The Fermi levels are shown at zero energy in both TDOS and PDOS. Any non-zero states observed in the Fermi levels indicate the metallic nature of these IMCs. The electronic property indicates that the Ni_3Sn_4, $Ni_{2.5}Cu_{0.5}Sn_4$, $Ni_{2.0}Cu_{1.0}Sn_4$, and $Ni_{1.5}Cu_{1.5}Sn_4$ phases exhibit metallic properties.

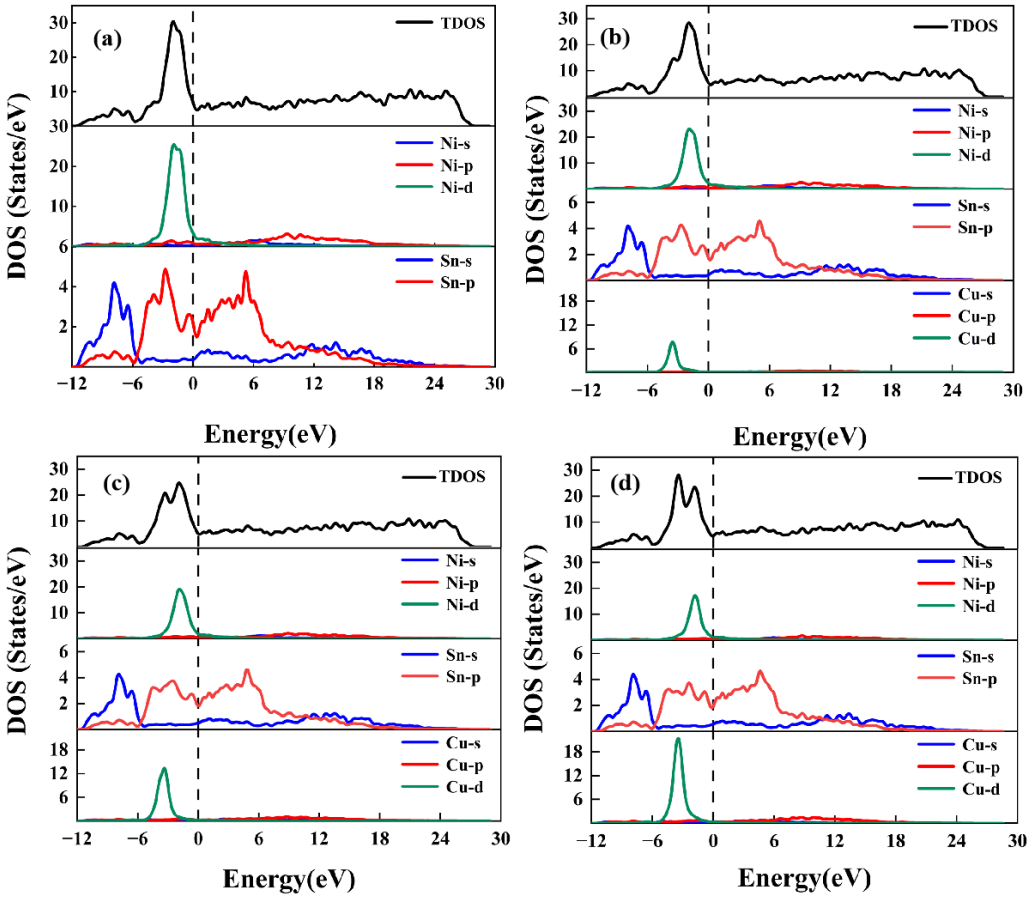

Figure 7. TDOS and PDOS for (**a**) Ni_3Sn_4, (**b**) $Ni_{2.5}Cu_{0.5}Sn_4$, (**c**) $Ni_{2.0}Cu_{1.0}Sn_4$, (**d**) $Ni_{1.5}Cu_{1.5}Sn_4$.

As shown in Figure 7a, the TDOS in the energy range of about −12 to −6 eV is predominantly contributed by the Sn-s state. In the region from about −6 eV to the Fermi level, the dominant parts of the TDOS are the Ni-d state and the Sn-p state. It is evident that the Ni-d states, which have undergone a slight hybridisation with the Sn-p states, form the primary component close to the Fermi level in Ni_3Sn_4. Compared to the Ni_3Sn_4 phase, the peak of the TDOS from −6 eV to the Fermi level has a reduced height as shown in Figure 7b–d. The Fermi level reflects the stability of the material. Material stability decreases as the TDOS value increases [42]. The TDOS for $(Ni,Cu)_3Sn_4$ structures is primarily influenced by Ni-d and Cu-d states. The relationship between the electronic structure and the ductility and brittleness of crystal structures is well established [43]. The strength of atomic interactions can be inferred from the overlap region of d- and p-hybridised orbitals. The addition of Cu atoms can increase the brittleness of Ni_3Sn_4. Furthermore, the d- and p-hybridised area gradually increases with the increase in Cu content.

This suggests that the hybridisation between the Ni-d and Sn-p electrons was weakened after Cu replaced Ni in Ni_3Sn_4. In addition, a new peak appears from −6 eV to 0 eV, which is mainly dominated by Cu-d electrons. The peak position of the Cu-d state corre-

sponded to the position of the Sn-p saddle point at an energy level of about −4 eV. Therefore, the doped Cu atoms could not adapt to the loss of bonding between Sn and Ni. In short, the binding energy of Ni_3Sn_4 exceeded that of Ni_3Sn_4-based IMCs. It is well known that a higher binding energy corresponds to a stronger charge interaction [44], which leads to an increase in structural stability. The results may explain the difference in elastic properties observed between Ni_3Sn_4 and $Ni_{2.5}Cu_{0.5}Sn_4$, $Ni_{2.0}Cu_{1.0}Sn_4$, and $Ni_{1.5}Cu_{1.5}Sn_4$.

4. Conclusions

In this study, Ni_3Sn_4-based IMCs are modelled by first-principles calculations to investigate the crystal structures and mechanical properties, as well as the electronic properties of the substitution of Cu for Ni in Ni_3Sn_4. We use the predictions of the systematic work calculated from first principles. As the concentration of Cu atoms in the Ni_3Sn_4 cells increases, the bulk modulus values of $(Ni,Cu)_3Sn_4$ formed with different compositions decrease from 107.78 GPa to 87.84 GPa, the shear modulus decreases from 56.64 GPa to 45.08 GPa, and the elastic modulus decreases from 144.59 GPa to 115.48 GPa, indicating that the doping of Cu atoms into the Ni_3Sn_4 cells may adversely affect their mechanical properties and increase the possibility of microcracking at the interface during actual service. It is also found that the anisotropy of $(Ni,Cu)_3Sn_4$ is more pronounced than that of Ni_3Sn_4, with the highest anisotropy observed in $Ni_{2.0}Cu_{1.0}Sn_4$. The metallic properties of Ni_3Sn_4 and the $Ni_{2.5}Cu_{0.5}Sn_4$, $Ni_{2.0}Cu_{1.0}Sn_4$, and $Ni_{1.5}Cu_{1.5}Sn_4$ phases are revealed by electronic structure analysis. The total density of states (TDOS) for $(Ni,Cu)_3Sn_4$ structures is mainly influenced by Ni-d and Cu-d states. The addition of Cu atoms can increase the brittleness of Ni_3Sn_4. In addition, the region where d and p hybridisation occurs gradually increases with increasing Cu content. The electronic properties suggest that the binding energy between Ni and Sn atoms weakens with the addition of Cu atoms, resulting in a decrease in the elastic modulus. This research can serve as a valuable reference and theoretical guide for future applications of these materials.

Author Contributions: Conceptualisation, J.Y. and H.M. (Haitao Ma); Methodology, X.L., X.C. and M.S.; Software, J.Y., L.W. and S.G.; Resources, H.M. (Haitao Ma); Data curation, J.Y., L.W., S.G., X.L., X.C., M.S. and H.M. (Haoran Ma); Writing—original draft, J.Y.; Supervision, H.M. (Haitao Ma); Funding acquisition, H.M. (Haoran Ma). All authors have read and agreed to the published version of the manuscript.

Funding: This work was supported by the National Natural Science Foundation of China (Grant No. 52101035).

Data Availability Statement: The data presented in this study are available on request from the corresponding author. The data are not publicly available due to privacy.

Conflicts of Interest: The authors declare no conflicts of interest.

References

1. Le, F.; Lee, S.R.; Zhang, Q. 3D chip stacking with through silicon-vias (TSVs) for vertical interconnect and underfill dispensing. *J. Micromech. Microeng.* **2017**, *27*, 45012. [CrossRef]
2. Cao, K.; Zhou, J.; Wei, T.; Chen, M.; Hu, S.; Li, K. A survey of optimization techniques for thermal-aware 3D processors. *J. Syst. Archit.* **2019**, *97*, 397–415. [CrossRef]
3. Ma, H.R.; Kunwar, A.; Shang, S.Y.; Jiang, C.R.; Wang, Y.P.; Ma, H.T.; Zhao, N. Evolution behavior and growth kinetics of intermetallic compounds at Sn/Cu interface during multiple reflows. *Intermetallics* **2018**, *96*, 1–12. [CrossRef]
4. Wang, J.; Chen, J.; Zhang, Z.; Zhang, P.; Yu, Z.; Zhang, S. Effects of doping trace Ni element on interfacial behavior of Sn/Ni (polycrystal/single-crystal) joints. *Solder. Surf. Mt. Technol.* **2021**, *34*, 124–133. [CrossRef]
5. Tu, K. *Solder Joint Technology*; Springer: Berlin/Heidelberg, Germany, 2007; Volume 117, pp. 7–11.
6. Tu, K.; Hsiao, H.; Chen, C. Transition from flip chip solder joint to 3D IC microbump: Its effect on microstructure anisotropy. *Microelectron. Reliab.* **2013**, *53*, 2–6. [CrossRef]
7. Pan, H.; Wang, Y.; Luo, W.; Gao, L.; Li, M. Effect of Ni thickness on the IMC and reliability of ultrathin ENEPIG. In Proceedings of the 2018 19th International Conference on Electronic Packaging Technology (ICEPT), Shanghai, China, 8–11 August 2018; pp. 667–671.

8. Jen, Y.; Chiou, Y.; Yu, C. Fracture mechanics study on the intermetallic compound cracks for the solder joints of electronic packages. *Eng. Fail. Anal.* **2011**, *18*, 797–810. [CrossRef]
9. Li, Q.; Zhao, W.; Zhang, W.; Chen, W.; Liu, Z. Research on thermal fatigue failure mechanism of BGA solder joints based on microstructure evolution. *Int. J. Fatigue* **2023**, *167*, 107356. [CrossRef]
10. Yang, C.; Le, F.; Lee, S.R. Experimental investigation of the failure mechanism of Cu–Sn intermetallic compounds in SAC solder joints. *Microelectron. Reliab.* **2016**, *62*, 130–140. [CrossRef]
11. Chen, H.; Chen, C. Kinetic study of the intermetallic compound formation between eutectic Sn–3.5 Ag alloys and electroplated Ni metallization in flip-chip solder joints. *J. Mater. Res.* **2012**, *27*, 1169–1177. [CrossRef]
12. Huang, C.; Jang, G.; Duh, J. Interfacial reactions and compound formation in the edge of PbSn flip-chip solder bumps on Ni/Cu under-bump metallization. *J. Electron. Mater.* **2003**, *32*, 1273–1277. [CrossRef]
13. Kumar, A.; Chen, Z.; Mhaisalkar, S.G.; Wong, C.C.; Teo, P.S.; Kripesh, V. Effect of Ni–P thickness on solid-state interfacial reactions between Sn–3.5 Ag solder and electroless Ni–P metallization on Cu substrate. *Thin Solid Film.* **2006**, *504*, 410–415. [CrossRef]
14. Hai, S.; Oh, S.; Yu, H. Evaluation of creep properties for aged Pb-free solder joints/(Ni-P/Au) UBM with small addition Cu using shear punch creep testing method. *Eng. Fail. Anal.* **2020**, *113*, 104558. [CrossRef]
15. Xiao, J.; Wang, F.; Li, J.; Chen, Z. Comparison of interfacial reactions and isothermal aging of cone Ni-P and flat Ni-P with Sn3. 5Ag solders. *Appl. Surf. Sci.* **2023**, *625*, 157219. [CrossRef]
16. Mitchell, D.; Guo, Y.; Sarihan, V. Methodology for studying the impact of intrinsic stress on the reliability of the electroless Ni UBM structure. *IEEE Trans. Compon. Packag. Technol.* **2001**, *24*, 667–672. [CrossRef]
17. Jeon, Y.; Paik, K.; Bok, K.; Choi, W.; Cho, C. Studies on Ni-Sn intermetallic compound and P-rich Ni layer at the electroless nickel UBM-solder interface and their effects on flip chip solder joint reliability. In Proceedings of the 2001 Proceedings, 51st Electronic Components and Technology Conference (Cat. No. 01CH37220), Orlando, FL, USA, 29 May–1 June 2001; pp. 1326–1332.
18. Chen, P.; Li, C.; Yang, C.; Hu, A.; Li, M.; Gao, L.; Ling, H.; Hang, T.; Wu, Y. Growth behavior of Ni-Sn intermetallic compounds in microbumps during long-term aging process. *Mater. Lett.* **2022**, *313*, 131743. [CrossRef]
19. Ji, H.; Li, M.; Ma, S.; Li, M. Ni_3Sn_4-composed die bonded interface rapidly formed by ultrasonic-assisted soldering of Sn/Ni solder paste for high-temperature power device packaging. *Mater. Design* **2016**, *108*, 590–596. [CrossRef]
20. Lin, C.; Jao, C.; Lee, C.; Yen, Y. The effect of non-reactive alloying elements on the growth kinetics of the intermetallic compound between liquid Sn-based eutectic solders and Ni substrates. *J. Alloys Compd.* **2007**, *440*, 333–340. [CrossRef]
21. He, H.; Huang, S.; Xiao, Y.; Goodall, R. Diffusion reaction-induced microstructure and strength evolution of Cu joints bonded with Sn-based solder containing Ni-foam. *Mater. Lett.* **2020**, *281*, 128642. [CrossRef]
22. Li, Z.; Cheng, K.; Liu, J.; He, Y.; Xiao, Y. Effect of Thermal aging on the interfacial reaction behavior and failure mechanism of Ni-xCu/Sn soldering joints under shear loading. *Materials* **2023**, *16*, 5253. [CrossRef]
23. Wang, Y.; Yang, J.; Huang, J.; Wang, W.; Ye, Z.; Chen, S.; Zhao, Y. First-principles calculations on physical properties of Ni_3Snx binary system intermetallic compounds and Ni/Ni_3Sn interfaces in Nickel-Tin TLPS bonding layer. *Intermetallics* **2018**, *101*, 27–38. [CrossRef]
24. Tian, Y.; Wu, P. First-Principles Study of Substitution of Au for Ni in Ni_3Sn_4. *J. Electron. Mater.* **2018**, *47*, 2600–2608. [CrossRef]
25. Jeitschko, W.; Jaberg, B. Structure refinement of Ni_3Sn_4. *Acta Crystallogr. Sect. B Struct. Crystallogr. Cryst. Chem.* **1982**, *38*, 598–600. [CrossRef]
26. Han, Y.; Chen, J.; Lin, M.; Zhang, K.; Lu, H. Synergistic effects of alloy elements on the structural stability, mechanical properties and electronic structure of Ni_3Sn_4: Using first principles. *Vacuum* **2023**, *214*, 112239. [CrossRef]
27. Zhang, W.W.; Ma, Y.; Zhou, W.; Wu, P. The Structural, Elastic and Electronic Properties of $Ni_{3-x}Cu_xSn_4$ (x = 0, 0.5, 1 and 1.5) Intermetallic Compounds via *Ab* Initio Calculations. *J. Electron. Mater.* **2019**, *48*, 4533–4543. [CrossRef]
28. Yao, P.; Liu, P.; Liu, J. Effects of multiple reflows on intermetallic morphology and shear strength of SnAgCu–xNi composite solder joints on electrolytic Ni/Au metallized substrate. *J. Alloys Compd.* **2008**, *462*, 73–79. [CrossRef]
29. Yao, P.; Liu, P.; Liu, J. Interfacial reaction and shear strength of SnAgCu–xNi/Ni solder joints during aging at 150 °C. *Microelectron. Eng.* **2009**, *86*, 1969–1974. [CrossRef]
30. Segall, M.D.; Lindan, P.J.; Probert, M.A.; Pickard, C.J.; Hasnip, P.J.; Clark, S.J.; Payne, M.C. First-principles simulation: Ideas, illustrations and the CASTEP code. *J. Phys. Condens. Matter* **2002**, *14*, 2717. [CrossRef]
31. Perdew, J.P.; Burke, K.; Ernzerhof, M. Generalized gradient approximation made simple. *Phys. Rev. Lett.* **1996**, *77*, 3865. [CrossRef] [PubMed]
32. Bi, X.; Hu, X.; Jiang, X.; Li, Q. Effect of Cu additions on mechanical properties of Ni_3Sn_4-based intermetallic compounds: First-principles calculations and nano-indentation measurements. *Vacuum* **2019**, *164*, 7–14. [CrossRef]
33. Bi, X.; Hu, X.; Li, Q. Effect of Co addition into Ni film on shear strength of solder/Ni/Cu system: Experimental and theoretical investigations. *Mater. Sci. Eng. A* **2020**, *788*, 139589. [CrossRef]
34. Beckstein, O.; Klepeis, J.E.; Hart, G.; Pankratov, O. First-principles elastic constants and electronic structure of $\alpha-Pt_2Si$ and PtSi. *Phys. Rev. B* **2001**, *63*, 134112. [CrossRef]
35. Nye, J.F. *Physical Properties of Crystals: Their Representation by Tensors and Matrices*; Oxford University Press: Oxford, UK, 1985; pp. 206–210.

36. Heciri, D.; Belkhir, H.; Belghit, R.; Bouhafs, B.; Khenata, R.; Ahmed, R.; Bouhemadou, A.; Ouahrani, T.; Wang, X.; Omran, S.B. Insight into the structural, elastic and electronic properties of tetragonal inter-alkali metal chalcogenides CsNaX (X = S, Se, and Te) from first-principles calculations. *Mater. Chem. Phys.* **2019**, *221*, 125–137. [CrossRef]
37. Cheng, H.; Yu, C.; Chen, W. First-principles density functional calculation of mechanical, thermodynamic and electronic properties of CuIn and Cu_2In crystals. *J. Alloys Compd.* **2013**, *546*, 286–295. [CrossRef]
38. Hill, R. The elastic behaviour of a crystalline aggregate. *Proc. Phys. Society. Sect. A* **1952**, *65*, 349. [CrossRef]
39. Pugh, S.F. XCII. Relations between the elastic moduli and the plastic properties of polycrystalline pure metals. *Lond. Edinb. Dublin Philos. Mag. J. Sci.* **1954**, *45*, 823–843. [CrossRef]
40. Hossain, K.M.; Mitro, S.K.; Rahman, M.M.; Khatun, A.A.; Parvin, F. Analyzing the physical properties of perovskite oxides $BaMO_3$ (M = Ru, Os) for predicting potential applications. *Comput. Condens. Matter* **2023**, *34*, e00782. [CrossRef]
41. Zeng, G.; Xue, S.; Zhang, L.; Gao, L.; Dai, W.; Luo, J. A review on the interfacial intermetallic compounds between Sn–Ag–Cu based solders and substrates. *J. Mater. Sci. Mater. Electron.* **2010**, *21*, 421–440. [CrossRef]
42. Eklund, C.; Fennie, C.J.; Rabe, K.M. Strain-induced ferroelectricity in orthorhombic $CaTiO_3$ from first principles. *Phys. Rev. B* **2009**, *79*, 220101. [CrossRef]
43. Gschneidner, K.A., Jr.; Ji, M.; Wang, C.Z.; Ho, K.M.; Russell, A.M.; Mudryk, Y.; Becker, A.T.; Larson, J.L. Influence of the electronic structure on the ductile behavior of B2 CsCl-type AB intermetallics. *Acta Mater.* **2009**, *57*, 5876–5881. [CrossRef]
44. Fu, C.L.; Wang, X.; Ye, Y.Y.; Ho, K.M. Phase stability, bonding mechanism, and elastic constants of Mo5Si3 by first-principles calculation. *Intermetallics* **1999**, *7*, 179–184. [CrossRef]